Influence of carbon content on the strength of cubic BC_xN: A first-principles study

Yi Zhang,[1,2] Hong Sun,[2,1] and Changfeng Chen[1]
[1]*Department of Physics and High Pressure Science and Engineering Center, University of Nevada, Las Vegas, Nevada 89154, USA*
[2]*Department of Physics, Shanghai Jiao Tong University, Shanghai 200030, China*
(Received 22 October 2007; revised manuscript received 26 January 2008; published 18 March 2008)

It has been widely expected that higher carbon content in ternary compounds BC_xN, which crystallize in cubic diamond structure, would lead to increased strength and hardness. This notion was derived from calculated elastic parameters and empirical hardness formulas based on structural and electronic properties of the equilibrium structures. Here we report on a first-principles study of cubic BC_6N that exhibits only slightly increased tensile strength, but decreased shear strength compared to cubic BC_2N. More important, both compounds show lower tensile and shear strength compared to cubic BN. We analyze these seemingly counterintuitive results and show that material strength is determined by mechanical response at large strains which may not always be in accordance with the properties of the equilibrium structure. Studies of stress-strain behavior at large deformation, as demonstrated in the present work, are required for a reliable account for material strength under various loading conditions.

DOI: 10.1103/PhysRevB.77.094120 PACS number(s): 62.20.−x, 71.15.Mb, 81.40.Jj

I. INTRODUCTION

In recent years considerable effort has been devoted to the synthesis and characterization of ternary BC_xN compounds that crystallize in cubic diamond (zinc-blende) structure.[1–12] The idea is to make new compounds that are a hybrid of diamond and cubic BN (*c*-BN), the top two known strongest solids, with the expectation that they will have the best of the two worlds in their mechanical properties—namely, stronger than *c*-BN and thermally more stable than diamond. It is also expected that higher carbon content would help increase the strength and hardness; this is based on the intuitive argument that more carbon content should bring the hybrid compounds closer to diamond in their mechanical properties because of the larger proportion of the stronger C-C bonds in the structure. A variety of structural forms of BC_xN were obtained under high-pressure and high-temperature synthesis conditions from different starting materials. The best characterized and most studied are two cubic BC_2N phases in the zinc-blende structure: a high-density phase[2,5] obtained from compressing a mixture of fine-milled graphite and graphitic BN and a low-density phase[4] from a graphitic BC_2N precursor. They show large differences in lattice constants and elastic parameters as probed by x-ray diffraction and equation of state (volume-pressure) measurements[2,4,5] and in lattice dynamics as probed by Brillouin scattering measurements.[6] Identation measurements[4,5] produced large (but different) hardness values for the two BC_2N phases, placing them in the superhard category with the measured hardness above that of *c*-BN. The difference in the measured hardness values is a reflection of the sensitive dependence of hardness on a large array of external and sometimes uncontrolled conditions, including the loading conditions (load and loading rate and configurations), indentor shape, and crack formation in the sample, among others. This is why the indentation hardness of a material is not uniquely defined and a comparison of absolute readings of hardness from different indentation experiments is often not very meaningful. Instead, relative hardness values obtained under the same measurement conditions are the desired information for useful comparison.[4,5] Nevertheless, there is a well-defined common underlying process that is key to understanding the structural deformation, strength, and hardness and can be tracked from first-principles calculations. It is the ideal strength of a material under specified loading conditions. It is defined as the stress at which a perfect crystal becomes mechanically unstable which sets an upper bound for material strength. A computational approach was devised[13,14] to determine the ideal strength from first-principles density functional theory calculations. It has been recently applied to examine diamond, *c*-BN, and BC_2N under tensile and shear strains.[15–19] The results shed light on the deformation mechanism of these materials and demonstrate that elastic parameters and other equilibrium structure properties do not provide a good indication for structural deformation at large strains. A limiting case of the BCN compounds is several polymorphs of C_3N_4, which have been considered as possible candidates for superhard materials due to their short C-N covalent bonds that give rise to the predicted high elastic moduli.[20–22] However, recent ideal strength studies[23,24] showed that the β- and pseudocubic C_3N_4, where the C-N bonds are formed by the sp^2 electron from N and sp^3 electron from C in the former and by the sp^3 electron from N and sp^3 electron from C in the latter, both are not as strong as *c*-BN since the calculated ideal tensile and shear strength are much lower than expected.

It was recently proposed[25] that a cubic BC_6N phase could exhibit higher strength and hardness than those of the isostructural cubic BC_2N. The calculated elastic parameters and hardness from structural and electronic properties of the equilibrium structure all point to the same conclusion. However, as seen in other similar B-C-N compounds,[15–19,23,24] these indicators from equilibrium structure properties may not offer a reliable assessment of the mechanical strength at large strains. Moreover, the detailed deformation modes and bond-breaking patterns, both critical to understanding the atomistic mechanism of the structural deformation, can only be obtained from the ideal strength calculations.

In this paper, we report the results of *ab initio* pseudopo-

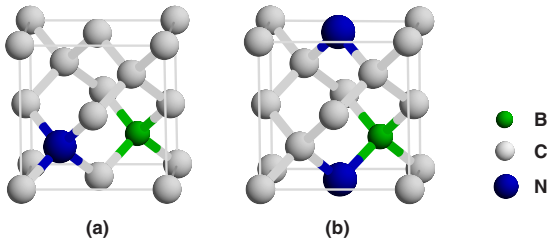

FIG. 1. (Color online) The two eight-atom zinc-blende-structured unit cells of BC_6N containing (a) no (BC_6N-1) or one (BC_6N-2) B-N bond.

tential local-density-approximation (LDA) calculations for BC_6N and compare the results to those of diamond, c-BN, and BC_2N to study the effect of increasing carbon content. The total energy, ground-state properties, elastic moduli, and ideal tensile and shear strength were calculated for a systematic comparison. The results show that despite the increased elastic moduli, BC_6N exhibits only slightly increased tensile strength well below the proportion of the carbon content increase. Furthermore, its shear strength even decreases compared to that of BC_2N. We examine the atomistic deformation modes and bond-breaking sequences in these compounds in close comparison with those in diamond and *c*-BN to unveil the underlying mechanism for these unexpected mechanical behavior at large strains. The results provide useful insights for understanding structural deformation of strong covalent materials and may also help understand similar behavior in other classes of materials.

II. STRUCTURAL MODEL AND METHOD OF CALCULATION

We consider the cubic BC_6N structures in an eight-atom zinc-blende-structured unit cell. Among $8!/6!=56$ possible structural configurations, there are only two topologically different structures as shown in Fig. 1. They are distinguished by the absence [BC_6N-1 in Fig. 1(a)] or presence [BC_6N-2 in Fig. 1(b)] of the B-N bond in the unit cell. The total energy of the system is calculated using a local-density-approximation pseudopotential scheme with a plane-wave basis set.[26–28] The normal conserving Troullier-Martins pseudopotentials[29] were used with cutoff radii of 1.3, 1.3, and 1.5 a.u. for N, C, and B, respectively. The exchange correction functional of Ceperley and Alder[27] as parametrized by Perdew and Zunger[30] was used. The total energy of the structure was minimized by relaxing the structural parameters using a quasi-Newton method.[31] The total energy and stress calculation used an $8\times8\times8$ Monkhorst-Pack *k*-point grid[32] and a 100-Ry energy cutoff. The error in stress caused by the energy cutoff and *k*-point grid is less than 0.1 GPa based on convergence tests. The bulk moduli are obtained by fitting the Birch-Murnaghan equation of state. To determine the elastic constants, we applied a series of positive and negative strains to the equilibrium structure with all the atoms in the unit cell fully relaxed. Since the relaxed cubic BC_6N structures are slightly deformed from cubic, we calculated the average tetragonal $[\overline{(C_{11}-C_{12})/2}]$ and rhombohedral $[\overline{C_{44}}]$ shear moduli.[12] The calculated structural and energetic properties of the two cubic BC_6N phases are presented in Table I. For comparison, calculated results for diamond, cubic BN, and a high-density phase of BC_2N, which exhibits the highest ideal strength among the cubic BC_2N phases in zinc-blende structure,[15] are also listed; these results are all in good agreement with available experimental data.[12,15,33] All the equilibrium properties of the two cubic BC_6N phases (some are not listed in Table I since they are not directly related to our discussion here) of cubic BC_6N obtained in our work are in good agreement with the recently reported results.[25] The only exception is that our calculated bulk modulus for BC_6N-2 is higher than that for BC_6N-1. We will address this issue below.

To calculate the ideal strength along different deformation paths, we employed the method described in detail previously.[13,14] The lattice vectors were incrementally deformed in the direction of the applied (tensile or shear) strain. At each step, the applied (tensile or shear) strain is fixed which determines the calculated (tensile or shear) stress, while the other five independent components of the strain tensors and all the atoms inside the unit cell were simultaneously relaxed until (i) all the residual components of the Hellmann-Feynman stress tensor orthogonal to the applied strain are less than 0.1 GPa and (ii) the force on each atom becomes negligible. The shape of the unit cell is deter-

TABLE I. Calculated structural, energetic, and elastic properties of cubic BC_6N. The results for diamond, cubic BN, and BC_2N are also listed for comparison. The average lattice constant $\bar{a}$ is defined as $(abc)^{1/3}$.

Structure	BC_6N-1	BC_6N-2	BC_2N	Diamond	*c*-BN
a (Å)	3.560	3.563	3.568	3.538	3.592
b (Å)	3.572	3.563	3.568	3.538	3.592
c (Å)	3.572	3.563	3.607	3.538	3.592
$\bar{a}$ (Å)	3.568	3.563	3.581	3.538	3.592
$-E_{tot}$ (eV/atom)	160.04	160.15	165.07	155.47	175.50
E_f (eV/atom)	0.441	0.325	0.420	—	—
B_0 (GPa)	412.7	421.8	400.8	459	393
$\overline{C_{44}}$ (GPa)	525.4	531.6	492.3	599	472
$\overline{(C_{11}-C_{12})/2}$ (GPa)	427.0	423.9	314.1	469	311

TABLE II. Calculated ideal tensile and shear strength for BC_6N-1 and BC_6N-2 compared to those of diamond, cubic BN, and BC_2N.

	Ideal tensile			Ideal shear		
Structure	Strength	Direction	Strain	Strength	Direction	Strain
BC_6N-1	62.1	$\langle 111\rangle$	0.170	65.8	$(111)\langle 11\bar{2}\rangle$	0.205
BC_6N-2	58.4	$\langle 111\rangle$	0.160	63.0	$(111)\langle 1\bar{2}1\rangle$	0.190
c-BC_2N	55.8	$\langle 111\rangle$	0.080	68.8	$(111)\langle 1\bar{2}1\rangle$	0.270
Diamond	92.8	$\langle 111\rangle$	0.130	96.3	$(111)\langle 11\bar{2}\rangle$	0.345
c-BN	65.6	$\langle 111\rangle$	0.110	70.5	$(111)\langle 1\bar{2}1\rangle$	0.360

mined by this constrained atomic relaxation without any imposed boundary conditions. The obtained total energies of the structures are fitted by smooth energy-strain curves. From these energy-strain fit curves, we adopted a previously described approach[34] to calculate the tensile stress $\sigma_T=[(1+\epsilon_E)/V(\epsilon_E)]\partial E/\partial\epsilon_E$, where ϵ_E is the engineering strain, and the shear stress $\sigma_S=[1/V(\epsilon_T)]\partial E/\partial\epsilon_T$, where ϵ_T is the true strain. The obtained results are in excellent agreement with those obtained from direct stress calculations. To identify the weakest tensile direction, we calculated the tensile stress along various crystallographic directions of the structures. The critical shear stress was then calculated by applying shear deformation in the easy slip plane perpendicular to the weakest tensile direction. We examined the stress-strain relation along the directions of high symmetry since the symmetry lowers the energy and leads to energetically favorable relaxation pathways for structural transformation or failure.

III. RESULTS AND DISCUSSION

A. Equilibrium properties

From data listed in Table I, it is seen that all the BC_xN ($x=2,6$) structures have positive formation energy defined as $E_f=E_{BC_xN}-(xE_{diamond}+2E_{BN})/(x+2)$ where diamond and c-BN are used as energy references for c-BC_xN. This result indicates that the c-BC_xN compounds are all metastable and tend to segregate into diamond and c-BN. However, these metastable structures synthesized under high-temperature and high-pressure conditions can be recovered at ambient conditions as demonstrated in experiments.[1–5] We notice that the relatively more stable BC_6N-2 is lower in formation energy than the c-BC_2N which is the most stable c-BC_2N among those with similar cubic structures.[12] It shows that increasing carbon content indeed lowers the formation energy and thereby reduces the trend toward the phase segregation. The average lattice constants of c-BC_6N (BC_6N-1 and BC_6N-2) are smaller than that of c-BC_2N, but within the scale between diamond and c-BN, in good agreement with the Vegard's law,[35] which predicts a linear relation between the lattice constants of alloys and the concentration of its constitutional elements. The bulk moduli of c-BC_6N are only slightly larger than that of c-BC_2N, while their tetragonal and rhombohedral shear moduli exhibit much more significant enhancement. This contrast originates from the different underlying mechanical processes. The bulk moduli measure material response to isotropic compression whereas the shear moduli to shape change involving bond compression and elongation. The different types of bonds in the high-density cubic phases studied in the present work have similar lengths. Our calculated bond lengths for C-C, C-N, and C-B bonds in BC_6N-1 and BC_6N-2 are 1.536 Å, 1.549 Å, 1.559 Å and 1.536 Å, 1.550 Å, 1.563 Å, respectively. According to an empirical relation between bulk moduli and bond length,[36] the bulk moduli should not change much with the increase of C-C bonds in these structures since there is little variation in the overall bond length distribution. On the other hand, these bonds behave quite differently when they are stretched and distorted. As a result, the strong C-C bonds can help improve the shear moduli more effectively. Such differences become more pronounced at large strains as shown below in the discussion of ideal strength calculations. Differences also arise between BC_6N-1 and BC_6N-2 in lattice constants, elastic moduli, and formation energy. This can be explained by the bond counting rule: BC_6N-1, which contains four C-N bonds and four B-C bonds in each unit-cell, is not as stable as BC_6N-2, which has some of the B-C and C-N bonds in BC_6N-1 replaced by the energetically more stable C-C and B-N bonds. Consequently, the lattice constant of BC_6N-2 is reduced, which leads to a slight increase in the bulk modulus B_0 and rhombohedral shear modulus $\underline{C_{44}}$, but a slight decrease in the tetragonal shear modulus $\underline{(C_{11}-C_{12})}/2$. The different responses of these elastic moduli to the carbon content variation are due to the differences in the corresponding structural deformation modes associated with specific elastic moduli.

B. Ideal strength and deformation modes

The calculated ideal tensile and shear strength, the corresponding strains at the peak stress values, and the weakest tensile and shear deformation directions for cubic BC_6N-1 and BC_6N-2 are summarized in Table II. Also listed for comparison are the results for diamond, cubic BN, and an isostructural high-density cubic BC_2N phase. We first examine the stress-strain relations under tensile loading along high-symmetry paths, including all the body-diagonal, surface-diagonal, and lattice vectors of the cubic unit cell for all the materials considered here. The obtained ideal tensile strength of diamond, c-BN, and BC_2N are 92.9 GPa, 65.6 GPa, and

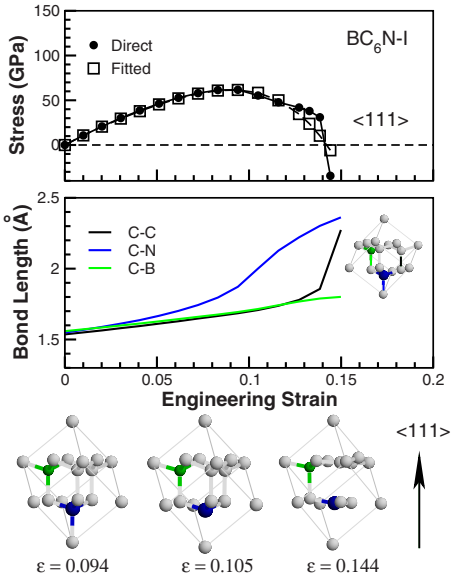

FIG. 2. (Color online) Calculated stress-strain relation, bond length versus strain, and the snapshots of the structural unit cell at the critical steps near the bond breaking points for BC_6N-1 under the ⟨111⟩ tensile loading. Solid circles and open squares represent results from the energy-strain fit and direct stress calculations, respectively.

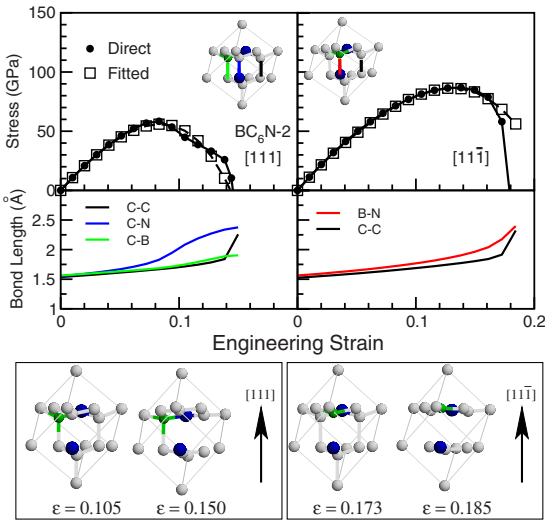

FIG. 3. (Color online) Calculated stress-strain relations, bond length versus strain, and the snapshots of the structural unit cell at the critical steps near the bond breaking points for BC_6N-2 under the [111] and [11$\bar{1}$] tensile loading. Solid circles and open squares represent results from the energy-strain fit and direct stress calculations, respectively.

55.8 GPa, respectively, all in the ⟨111⟩ crystallographic direction. For BC_6N-1, the calculated peak tensile stresses along the [001], [011], and [111] directions are 187.9 GPa, 96.2 GPa, and 62.1 GPa, respectively. Since all the body-diagonal directions in BC_6N-1 are equivalent, we identify the ⟨111⟩ directions as the weakest tensile direction with an ideal tensile strength of 62.1 GPa. The calculated peak stresses of BC_6N-2 along the [001] and [011] are 131.3 GPa and 93.2 GPa, respectively. However, there are two nonequivalent body-diagonal directions for BC_6N-2—namely, its [111] and [11$\bar{1}$] directions. These two directions can be distinguished by the orientation of the B-N bond, which is parallel to the [11$\bar{1}$] direction and perpendicular to the [111] direction. The peak stresses for the [111] and [11$\bar{1}$] directions are 58.4 GPa and 86.8 GPa, respectively. As a result, we identify the [11$\bar{1}$] as the weakest tensile direction for BC_6N-2 with an ideal tensile strength of 58.4 GPa. It is clear that an additional 24.5 wt % of carbon content in BC_6N over that in BC_2N only leads to no more than 11% of enhancement to its ideal tensile strength. Moreover, even with this modest increase the ideal tensile strength of c-BC_6N is still below that of c-BN.

To better understand the calculated ideal tensile strength results, we examine the detailed local bonding arrangements and atomistic deformation modes under tensile loading for c-BC_6N. In BC_6N-1 (see Fig. 2), there are two C-C bonds, one C-N bond, and one B-C aligned in the ⟨111⟩ direction. These bonds are primarily responsible for the strength under the ⟨111⟩ tensile loading because the tensile strain directly stretches these bonds, causing bond breaking and structural deformation. The stress undergoes an almost linear increase up to the maximum point (ϵ=0.09) where all the bonds remain intact but the C-N bond is significantly stretched. At further increased strain, the C-N bond breaks and the stress starts to fall. The break of the two C-C bonds occurs around the tensile strain of 0.135 with a drastic change of bond length from 1.84 Å to 2.26 Å. At this point, only the B-C bond remains connected and the stress turns negative immediately afterwards, indicating that the repulsive stress is pushing the structure away from equilibrium. Meanwhile, in BC_6N-2 (see Fig. 3), the types of bonds parallel to the [111] direction are the same as those parallel to ⟨111⟩ in BC_6N-1, producing the peak stress in the [111] direction for BC_6N-2 similar to that in the ⟨111⟩ direction for BC_6N-1. The 5.5% disparity in their values comes from the subtle differences in local bonding environments. Meanwhile, there are three C-C bonds and one B-N bond aligned in the [11$\bar{1}$] direction in BC_6N-2. The strong sp^3 C-C bonds produce a much larger tensile strength that is only slightly lower than the value for diamond. However, the anisotropic mechanical response of BC_6N-2 to tensile loading means that its ideal tensile strength is determined by the lower value of 58.4 GPa. The weakest tensile direction also determines the natural cleavage plane that is perpendicular to it. Similar to the situation for BC_6N-1, the tensile deformation along the [111] direction of BC_6N-2 has two bond-breaking steps in the sequence of C-N bond and then C-C bond. Meanwhile, in the [11$\bar{1}$] deformation, the B-N bond breaks first at the strain of ϵ =0.16 after a long continual elongation; it is followed by a sudden break of the three equivalent C-C bonds which leads to a steep drop in tensile stress. The contribution from these strong carbon bonds is the key to the large tensile strength in the [11$\bar{1}$] direction.

We now examine the stress-strain relation of c-BC_6N under shear deformation. Several shear directions in the easy-

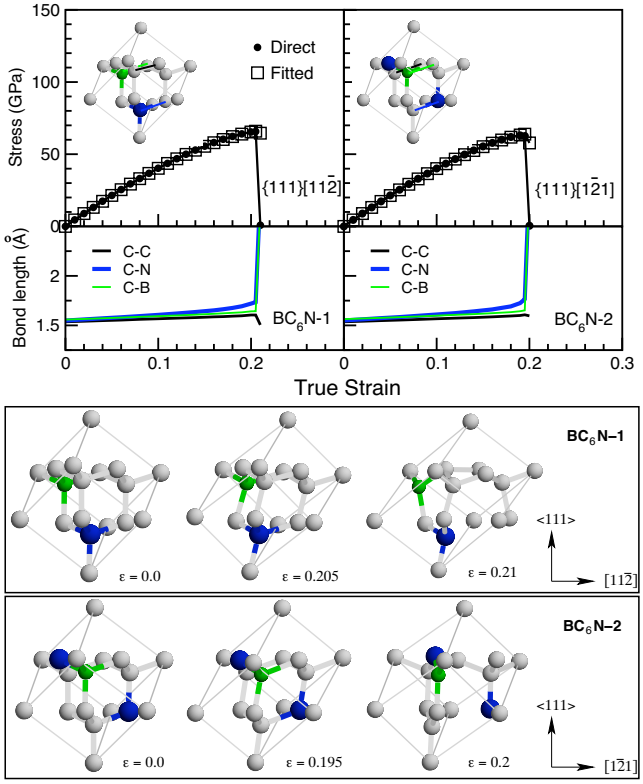

FIG. 4. (Color online) Calculated stress-strain relations, bond length versus strain, and the snapshots of the structural unit cell at the critical steps near the bond breaking points for BC_6N-1 and BC_6N-2 under the indicated shear loading. Solid circles and open squares represent results from the energy-strain fit and direct stress calculations, respectively.

slip ⟨111⟩ (for BC_6N-1) and [111] (for BC_6N-2) planes were checked. The ideal shear strengths of BC_6N-1 and BC_6N-2 are determined to be 65.8 GPa and 63.0 GPa along the {111}[11$\bar{2}$] and (111)[1$\bar{2}$1] directions, respectively. These values are below those for c-BN and c-BC_2N (see Table II). Since indentation hardness measurements produce volume and shape changes beneath the indenter, it is expected that shear strength is more closely related to the intrinsic hardness of a material. In fact, it has been shown that the limit of the structural stability is correlated with the maximum shear strength.[37] Our ideal shear strength calculations indicate that c-BC_6N is likely to be less hard compared to c-BN or c-BC_2N despite its increased carbon content. We examine the atomistic structural deformation modes to understand this result. Figure 4 shows the calculated stress-strain relations and the lengths of the bonds that connect the shear planes as a function of strain; the structural snapshots of the unit cell at the critical steps near the bond-breaking points are also plotted. It is seen that BC_6N-1 and BC_6N-2 are significantly deformed right before the bond-breaking points at the strain of ϵ=0.205 and ϵ=0.195, respectively. The C-N, C-C, and C-B bonds originally perpendicular to the [111] direction are greatly stretched, similar to the case in c-BC_2N,[15] However, the shear deformation modes for c-BC_6N are different from those in diamond, c-BN, and c-BC_2N in one regard. The latter three materials all the relevant bonds connecting the

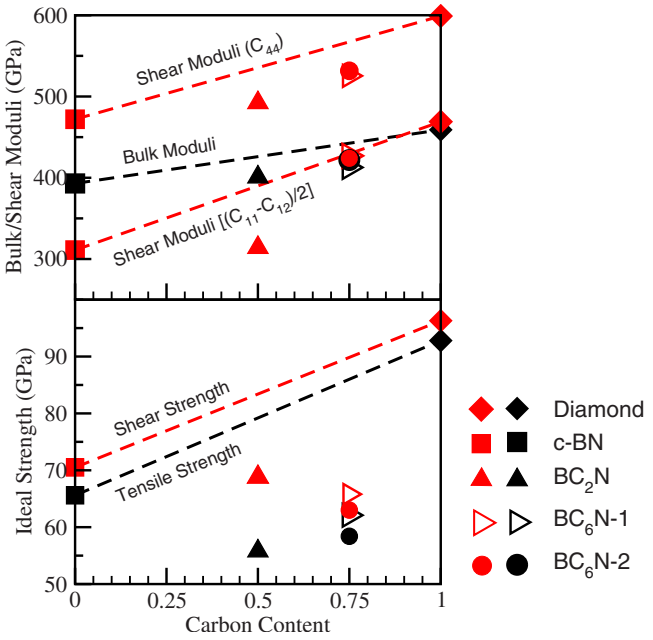

FIG. 5. (Color online) Summary of calculated bulk and shear moduli and ideal tensile and shear strength of the cubic BC_6N phases in comparison with the results for diamond, cubic BN, and BC_2N. The dashed lines represent linear interpolations between the data for c-BN and diamond.

shear planes break simultaneously, producing large peak shear stress.[16] However, in BC_6N-1 and BC_6N-2, the C-N and C-B bond-break at the peak stress point without much participation of the C-C bond. This early partial breakdown of chemical bonds in c-BC_6N is the weak link that is responsible for their reduced ideal shear strength. The increased number of stronger C-C bonds contribute to larger elastic moduli and lead to higher estimated hardness from empirical formulas derived from the equilibrium properties that is proportional to carbon content. All these cannot prevent structural deformation and failure of cubic BC_6N at its weak link mentioned above, and this weak link is not proportional to carbon content.

We present a summary of our calculated elastic moduli and ideal tensile and shear strength in Fig. 5 and compare them against the linear interpolation between cubic BN and diamond. It is seen that the elastic moduli follow the interpolation line (Vegard's law) quite well: all the calculated moduli show the correct trend in that more carbon content leads to higher moduli; the quantitative agreement is also very good (within a few percent in most cases). On the other hand, the calculated ideal strength deviates significantly from the interpolation: first, the values are much lower (20%–30%) than the interpolation line and, more significant, both the ideal tensile and shear strength turn lower from cubic BN to BC_2N and then, for the shear strength, this opposite (to Vegard's law) trend continues to BC_6N. This can be explained by the distribution of various bonds in these structures and their response to large strains as discussed above. The key to understanding this phenomenon is the realization that structure failure occurs when the weakest bonds break under specific deformation modes despite the larger proportion of stronger C-C bonds in the structures.

IV. CONCLUSION

In conclusion, our first-principles calculations of ideal strength and deformation modes show that increasing carbon content in cubic BC_6N leads to a slight increase of its tensile strength, but a decrease of its shear strength compared to an isostructural cubic BC_2N. Both of these compounds show lower ideal tensile and shear strength compared to cubic BN. We elucidate the underlying mechanism for these unexpected results by examining the structural deformation modes and bond-breaking patterns at large tensile and shear strains where the weak bonds in the tensile directions and those connecting the shear planes lead to structural instabilities. Given the prominent role played by the shear deformation and strength in indentation hardness measurements, it is expected that cubic BC_6N is not likely to be harder than its isostructural counterpart with reduced carbon content—namely, cubic BC_2N and BN. This is in strong contrast to the corresponding elastic moduli that show a significant increase with a larger amount of carbon content. This result indicates that empirical estimates of material strength and hardness based on structural and electronic properties at equilibrium may not be reliable when the bonding environment becomes complicated despite their successful applications to relatively simple materials. Meanwhile, it should be noted that the ideal strength is not equivalent to hardness, although they are closely related. Incorporating results from ideal strength calculations into the evaluation of material hardness is expected to provide more accurate predictions; but how to construct a simple and reliable formula for this purpose remains to be worked out.

ACKNOWLEDGMENTS

This work was supported by U.S. Department of Energy Cooperative Agreement No. DE-FC52-06NA26274 at UNLV. H.S. was also supported by NNSFC Grants Nos. 10574089 and 50532020 and the Chinese National Minister of Education Program for Innovative Research Team in University.

[1] S. Nakano, M. Akaishi, T. Sasaki, and S. Yamaoka, Chem. Mater. **6**, 2246 (1994).
[2] E. Knittle, R. B. Kaner, R. Jeanloz, and M. L. Cohen, Phys. Rev. B **51**, 12149 (1995).
[3] T. Komatsu, M. Nomura, Y. Kakudate, and S. Fujiwara, J. Mater. Chem. **6**, 1799 (1996).
[4] V. L. Solozhenko, D. Andrault, G. Fiquet, M. Mezouar, and D. Rubie, Appl. Phys. Lett. **78**, 1385 (2001).
[5] Y. Zhao, D. W. He, L. L. Daemen, T. D. Shen, R. B. Schwarz, Y. Zhu, D. L. Bish, J. Huang, J. Zhang, G. Shen, J. Qian, and T. W. Zerda, J. Mater. Res. **17**, 12 (2002).
[6] S. N. Tkachev, V. L. Solozhenko, P. V. Zinin, M. H. Manghnani, and L. C. Ming, Phys. Rev. B **68**, 052104 (2003).
[7] W. R. L. Lambrecht and B. Segall, Phys. Rev. B **40**, 9909 (1989).
[8] Y. Tateyama, T. Ogitsu, K. Kusakabe, S. Tsuneyuki, and S. Itoh, Phys. Rev. B **55**, R10161 (1997).
[9] J. C. Zheng, C. H. A. Huan, A. T. S. Wee, R. Z. Wang, and Y. M. Zheng, J. Phys.: Condens. Matter **11**, 927 (1999).
[10] R. Q. Zhang, K. S. Chan, H. F. Cheung, and S. T. Lee, Appl. Phys. Lett. **75**, 2259 (1999).
[11] M. Mattesini and S. F. Matar, Comput. Mater. Sci. **20**, 107 (2001).
[12] H. Sun, S. H. Jhi, D. Roundy, M. L. Cohen, and S. G. Louie, Phys. Rev. B **64**, 094108 (2001).
[13] D. Roundy, C. R. Krenn, M. L. Cohen, and J. W. Morris, Jr., Phys. Rev. Lett. **82**, 2713 (1999).
[14] D. Roundy, C. R. Krenn, M. L. Cohen, and J. W. Morris, Jr., Philos. Mag. A **81**, 1725 (2001).
[15] Y. Zhang, H. Sun, and C. F. Chen, Phys. Rev. Lett. **93**, 195504 (2004).
[16] Y. Zhang, H. Sun, and C. F. Chen, Phys. Rev. Lett. **94**, 145505 (2005).
[17] Y. Zhang, H. Sun, and C. F. Chen, Phys. Rev. B **73**, 144115 (2006).
[18] Z. C. Pan, H. Sun, and C. F. Chen, Phys. Rev. Lett. **98**, 135505 (2007).
[19] Z. C. Pan, H. Sun, and C. F. Chen, Phys. Rev. B **73**, 214111 (2006).
[20] A. Y. Liu and M. L. Cohen, Science **245**, 841 (1989).
[21] A. Y. Liu and M. L. Cohen, Phys. Rev. B **41**, 10727 (1990).
[22] A. Y. Liu and R. M. Wentzcovitch, Phys. Rev. B **50**, 10362 (1994).
[23] Y. Zhang, H. Sun, and C. F. Chen, Phys. Rev. B **73**, 064109 (2006).
[24] Y. Zhang, H. Sun, and C. F. Chen, Phys. Rev. B **76**, 144101 (2007).
[25] X. G. Luo, X. J. Guo, Z. Y. Liu, J. L. He, D. L. Yu, and Y. J. Tian, J. Appl. Phys. **101**, 083505 (2007).
[26] J. Ihm, A. Zunger, and M. L. Cohen, J. Phys. C **12**, 4409 (1979).
[27] D. M. Ceperley and B. J. Alder, Phys. Rev. Lett. **45**, 566 (1980).
[28] M. L. Cohen, Phys. Scr. **T1**, 5 (1982).
[29] N. Troullier and J. L. Martins, Phys. Rev. B **43**, 1993 (1991).
[30] J. P. Perdew and A. Zunger, Phys. Rev. B **23**, 5048 (1981).
[31] B. G. Pfrommer, M. Cote, S. G. Louie, and M. L. Cohen, J. Comput. Phys. **131**, 233 (1997).
[32] H. J. Monkhorst and J. D. Pack, Phys. Rev. B **13**, 5188 (1976).
[33] Z. C. Pan, H. Sun, and C. F. Chen, Phys. Rev. B **70**, 174115 (2004).
[34] W. Luo, D. Roundy, M. L. Cohen, and J. W. Morris, Jr., Phys. Rev. B **66**, 094110 (2002).
[35] L. Vegard, Z. Phys. **5**, 17 (1921).
[36] Y. He, C. Jayaprakash, and C. Rottman, Phys. Rev. B **32**, 12 (1985).
[37] A. Gouldstone, H. J. Koh, K. Y. Zeng, A. E. Giannakopoulos, and S. Suresh, Acta Mater. **48**, 2277 (2000).